LBL-20614
UC-95d

TEST, EVALUATION, AND REPORT ON MERCURY ENRICHMENT FOR FLUORESCENT LAMPS

J. Maya, M. Grossman, R. Lagushenko,
and P. Moskowitz

November 1985

Prepared for the U.S. Department of Energy under Contract DE-AC03-76SF00098

LBL-20614
EEB-L 85-09
L-106

TEST, EVALUATION, AND REPORT ON MERCURY ENRICHMENT FOR FLUORESCENT LAMPS

Jakob Maya, Principal Investigator*
M. Grossman, R. Lagushenko, and P. Moskowitz, Contributors*

Lighting Systems Research
Lawrence Berkeley Laboratory
University of California
Berkeley, CA 94720

November 1985

This work was supported by the Assistant Secretary for Conservation and Renewable Energy, Office of Buildings and Community Systems, Buildings Equipment Division of the U.S. Department of Energy under Contract No. DE-AC03-76SF00098.

* GTE Lighting Products
100 Endicott Street
Danvers, MA 01923

Subcontract No. 4524210

TEST, EVALUATION AND REPORT ON MERCURY ENRICHMENT FOR FLUORESCENT LAMPS

ABSTRACT

This report summarizes results of fluorescent lamp studies carried out during the time period Jan. 1, 1984 to Dec. 31, 1984 by GTE Products corporation for the DOE under a subcontract from Lawrence Berkeley Laboratories. The studies are divided into the following four areas: Magnetic Field Effects, Lamp Isotope Experiments, Modeling of Isotope Effects, and ^{196}Hg Isotope Separation in a Flow Reactor.

In the previous annual report we mentioned preliminary results utilizing transverse magnetic fields with fluorescent lamps. Here effects of both axial and transverse magnetic fields are studied in more detail and under controlled lamp operating conditions. Effects of changes in the Hg isotopic distribution are also studied here but specifically for uncoated fluorescent lamps in which emitted U.V radiation is measured. Monte-Carlo calculations were carried out to model the 253.7nm radiation transport process through a F40T/12 lamp. Solutions of the Holstein-Biberman equation were utilized to match the measured U.V. hfs and determine the near resonant energy transfer cross section. Finally, isotope separation process development continued with the goal of obtaining a reproducible high enrichment process. Substaintial progress was also made in developing diagnostics for the enrichment process.

ACKNOWLEDGEMENTS

The continued support, interest and encouragement of Dr. S. Berman from Lawrence Berkeley Laboratory and of Dr. J.F. Waymouth from GTE is gratefully acknowledged.

Many of the magnetic field experiments, both transverse and axial, have been carried out by Dr. Philip Moskowitz of our laboratory. Much of the Monte-Carlo work has been undertaken under the guidance and interest of Professor James B. Anderson of University of Pennsylvania. The able help of Mr. William George and the personnel at our "Test and Measurements" facility is gratefully acknowledged.

This work was supported by the Assistant Secretary for Conservation and Renewable Energy, Office of Buildings and Community Systems, Buildings Equipment Division of the U.S. Department of Energy under Contract No. DE-AC03-76SF00098.

CONTENTS

I. ANNUAL REPORT HIGHLIGHTS

1. A variety of lamps have been subjected to transverse and axial magnetic fields. Integrating sphere measurements in temperature controlled environment indicated 1-10% increases in LPW for magnetic field strengths of 0-400 Gauss.

2. We have carried out radial U.V. and visible light distribution measurements across the tube diameter as a function of magnetic field. We have observed substantial changes in radial light distribution for both axial and transverse magnetic fields. This suggests the necessity for extreme care in interpreting measurements outside the integrating sphere.

3. Waterbath U.V. measurements on an F40T/12 quartz fluorescent lamp indicated 6.8% improvement in U.V. output/arc watt with 2.6% ^{196}Hg. This is in good agreement with total light output integrating sphere measurements when end losses of the latter are taken into account.

4. Fabry-Perot measurements of the hyperfine structure of the 253.7nm line for lamps with natural as well as ^{196}Hg enriched mercury as a function of cold spot temperature have been completed.

5. A modified Holstein-Biberman formalism to calculate the hyperfine structure of the 253.7nm line has been developed. This formalism has been used to predict the hyperfine structure as well as efficiency improvements due to isotopic alteration in lamps.

6. As an alternative approach, a Monte-Carlo formalism has been developed and applied to calculate the line shape as well as efficiency improvements in fluorescent lamps.

7. In isotope separation experiments a lamp-filter combination with temperature controlled cold spots and lamp side walls has been designed, constructed and tested to characterize the emission. This enabled us to obtain reproducible and controllable U.V. photon flux to activate the photochemical reaction.

8. A 253.7nm transmission probe has been designed, constructed and put into use to obtain quantitative information about mercury transport down the photochemical reactor and utilization factor of the mercury flow through the system. This probe, placed downstream from the reactor monitors changes in line of sight Hg density under different operating conditions.

9. A continuous process, starting from natural Hg, proceeding to enriched Hg, recovering and dispensing this mercury and proceeding to a finished lamp with improved efficiency has been designed and successfully implemented.

10. Using the photochemical isotope separation technique single pass enrichment factors up to 32 have been demonstrated. Reproducibility of the high enrichment runs has been verified and optimization procedures established.

11. 30 percent utilization of the feedstock ^{196}Hg has been achieved for high enrichment runs.

II. MAGNETIC FIELD EFFECTS

Recent work of Richardson and Berman[1] and Ingold and Roberts[2] indicate local efficacy improvements in fluorescent lamps due to application of magnetic fields. These results, however, lacked either temperature control and/or uniform magnetic field measurements in integrating spheres. Due to alteration of discharge cross section under magnetic field conditions it is important to run efficacy measurements inside the integrating sphere.

We have carried out a number of experiments to investigate, in a controlled manner, the effects of magnetic fields on lamp efficiency. Local emission measurements took place whereby radiation from only one section of the lamp and from a restricted solid angle was detected. Both U.V. (253.7nm) emission and emission from phosphor coated lamps was measured in this way. In addition to local measurements integrating sphere measurements were carried out which permitted detection over 4π steradians. Both axial and transverse (relative to positive column orientation) externally applied magnetic fields were investigated as well as a number of different length and diameter lamps. As will be shown below very significant improvement in lamp efficiency can be obtained with proper use of magnetic fields.

Localized Magnetic Field Measurements

Experiments on an uncoated F40T/12 lamp were carried out with the lamp inserted in a Helmholtz coil magnetic field that extended approximately 3" along the lamp positive column. The emission of 253.7nm radiation both perpendicular and parallel to the transverse magnetic field was measured with a double monochromator. A view of the set up is shown in Figure 1.

Figure 1. Localized UV Output for F40T/12
Lamp in Transverse B Field

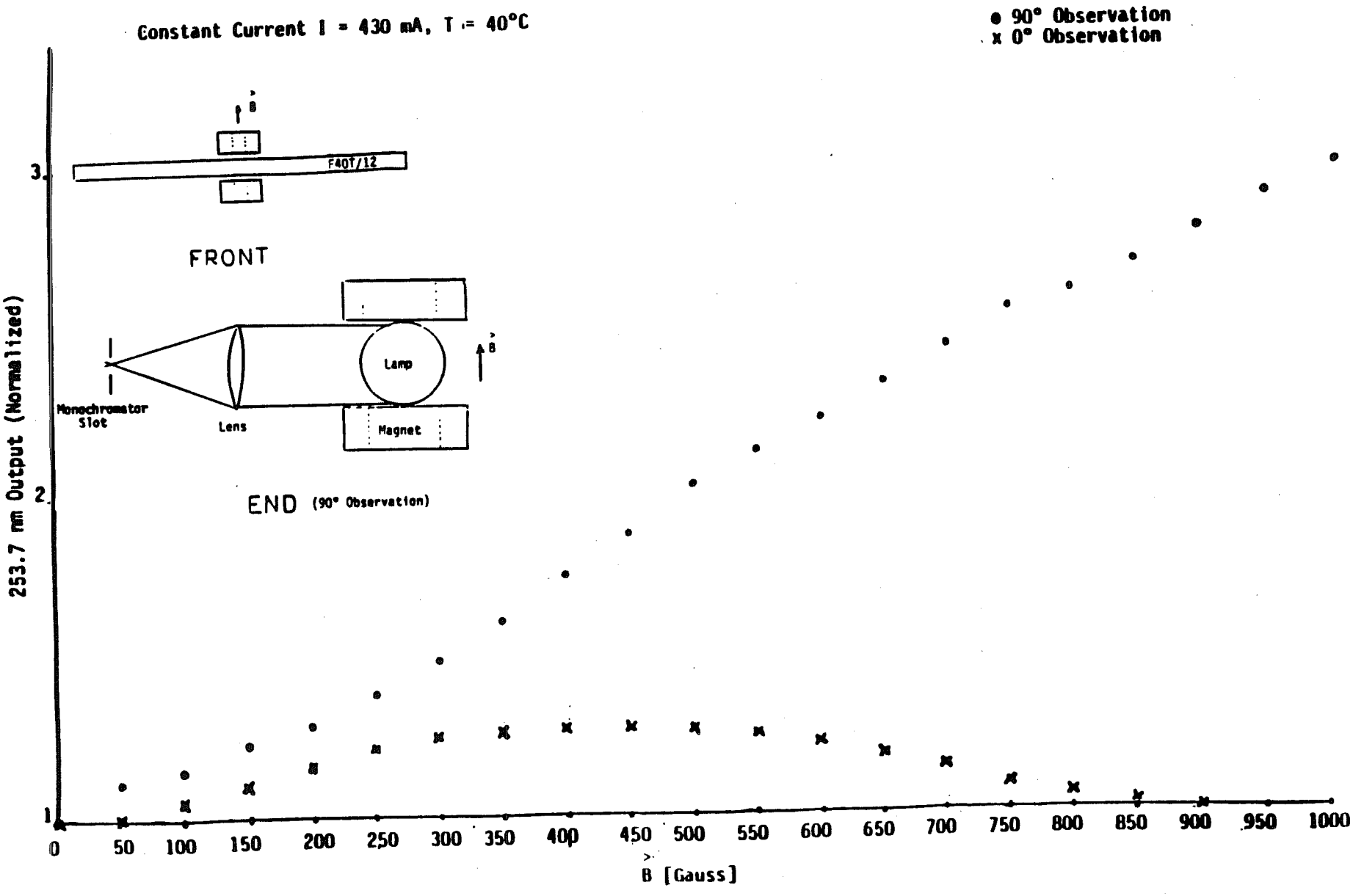

The lamp was operated under standard conditions that is, an arc current of 430 mA, and a lamp envelope temperature of $40^{o}C$. This temperature was maintained through the use of a water jacket. Some data was also taken at a constant lamp power of 38.5 arc watts.

The uniformity of the transverse magnetic field was measured and was found to be about 20% larger at the tube walls than at the center. Values appearing in the data refer to the center field at the lamp center.

The lamp was operated for about 1 hour before the data in Figure 1 was recorded. The ordinate is normalized emission, that is, U.V. emission over U.V. emission at zero field. Note the maximum at about 500 gauss for observation parallel to the field.

From a visual observation of the lamp, the increase in U.V. emission perpendicular to the field is due to an enhanced concentration of plasma in a region near the lamp wall.

Figure 2 shows the normalized U.V. efficiency for an F40T/12 lamp in an axially symmetric magnetic field. Localized increases of 10% at about 400 gauss have been observed. This is not an overall efficiency improvement because we have not, for example, measured all the light at other points.

In an effort to subject a greater portion of the discharge to a magnetic field, a special F4T/5 U.V. glass lamp was fabricated, and U.V. efficiency measurements similar to those carried out for the F40T/12 were performed. In this case, the magnetic field permeates the entire lamp structure, including the electrodes, although it is by no means uniform. Two identical Helmholtz coils were used here, resulting in maximum field intensities at the electrodes for the axial field case. Figure 3 shows

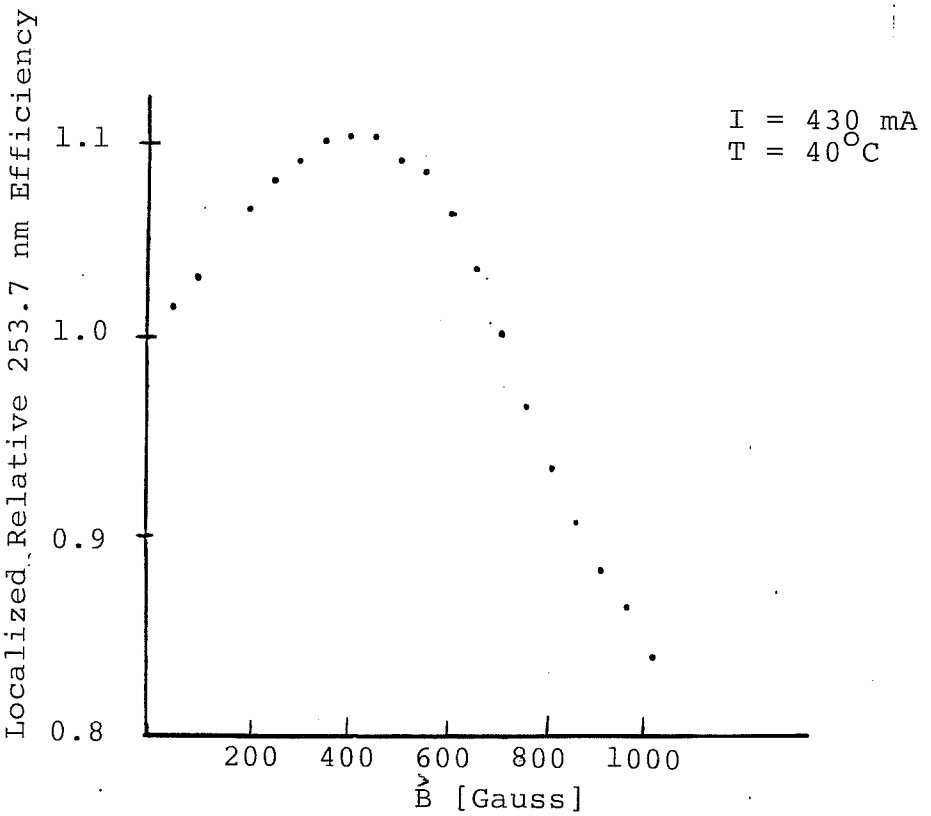

Figure 2. Localized UV Output per watt for F40T/12 Lamp in Axial B Field

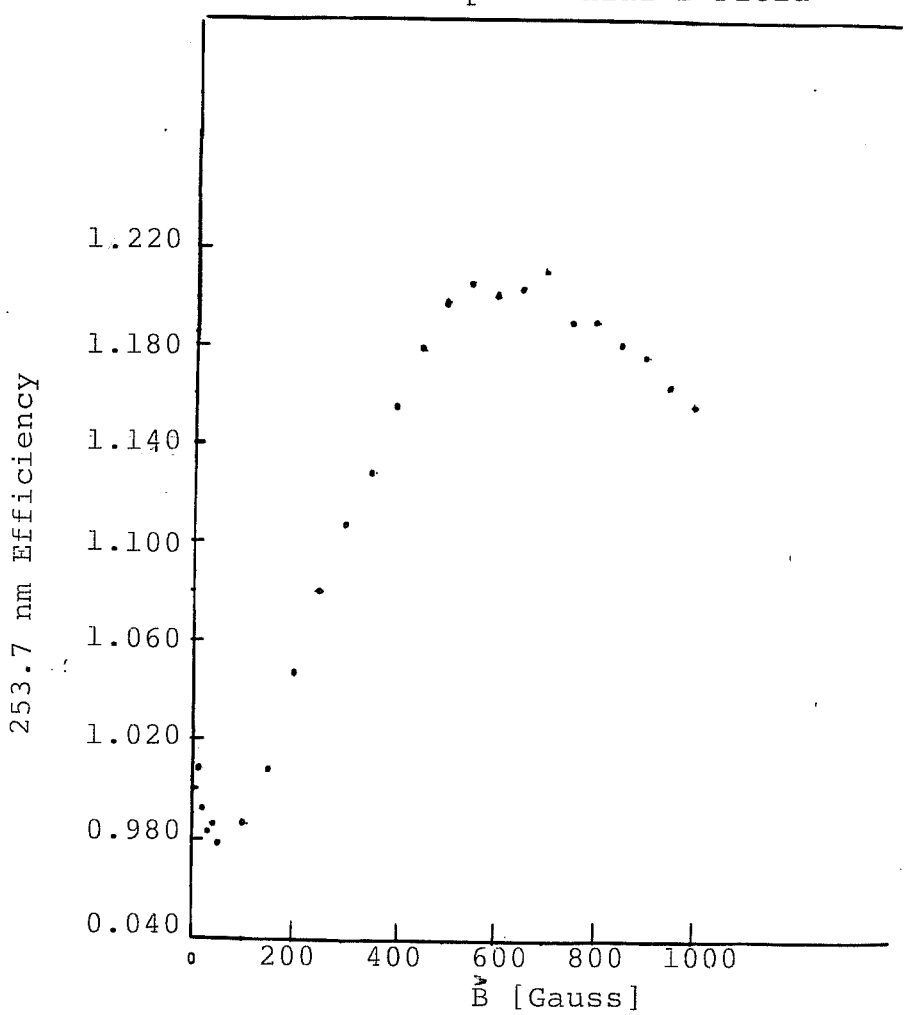

Figure 3. Localized UV Output per watt for F4T/5 lamp, Axial B Field

normalized U.V. efficacy at 253.7 nm versus "center field" strength. Note the local 21% increase at about 625 gauss. The lamp was operated at the standard current of 170 mA and an envelope temperature of $40^{o}C$.

By probing the lamp with a movable narrow slit and lens arrangement, U.V. efficiency versus distance from lamp center was measured. In the transverse field case, at 0 degree observation angle, the "spreading" of the arc plasma to the walls was verified.

The observed increases in lamp U.V. efficiency can be due to increases in electron temperature and/or decreases in photon trapping times. Probes of the spectral emission of an F4T/5 U.V. lamp from 240-640 nm will help in determining which of these mechanisms is responsible. Note that initial data show increases in line intensity for all the major mercury discharge components. Lineshape analysis with an interferometer will also shed light on this question.

Integrating Sphere Measurements

Integrating sphere measurements permit measurement of light emitted over 4π steradians from the entire lamp surface. Table 1 summarizes the integrating sphere measurements carried out.

Table 1
Summary of Integrating Sphere Measurements

Test No.	Lamp	Field Configuration	Field Strength	LPW Increase	Field Generation
1	F40T/12	Transverse	40G	2.2%	Permanent Magnet Strips
2	F40T/12	Transverse	110G	4%	Permanent Magnet Strips
3	F40T/12	Axial	275G	1%	Permanent Ring Magnets
4	G8T/5	Axial	0-400G	(10%)*	2 Helmholtz Coils Center
5	Bent T/5	Transverse	100G	6%	Bar magnets
6	F20T/12	Axial	0-100G	5%	7 Helmholtz coils

*253.7nm output/lamp watt increase.

The F40 lamp tests were conducted in a 2.5 meter sphere. For tests 1 and 2 the lamps had two flexible magnetized strips of square cross-section placed along the lamp on a diameter. The field lines penetrated the discharge as shown in Figure 4a. Field strengths quoted are those at the center of the discharge.

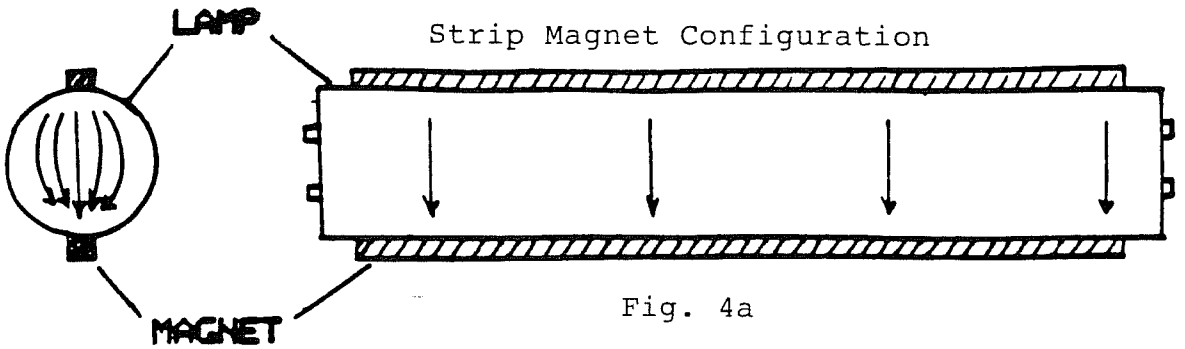

Fig. 4a

Fig. 4a

Note the 4% increase in LPW with the newly acquired stronger magnetic strips used in Test No. 2 as shown in Table 1. These tests were performed at constant 430 mA discharge current.

In Test No. 3, magnetized "rings" were fitted over both ends of an F40T/12 lamp, subjecting the coil region to an axial field. Of course, due to the dipole nature of the field, regions of the discharge surrounding the coil area experienced radial inward or outward directed fields. This yielded a 1% LPW increase.

The germicidal G8T/5 lamp was placed in a 1 meter sphere, with an adjustable field. Peak 253.7nm per lamp watt increase of 10% was recorded at 400 Gauss. This measurement differed from those above in that envelope wall temperature was controlled with a water jacket to 40^{o}C.

A magnetic field was produced inside a bent T/5 compact

fluorescent lamp producing a transverse magnetic field along most of the positive column. A linear reactor was used as a ballast. The linear reactor setting was kept constant during the course of the experiments and a 1.6 meter integrating sphere used to determine the absolute lumen output. At least 1 hour of stabilization time was used between each reading. As much as a 6% improvement in LPW relative to the normal lamp was found.

In order to create a more uniform magnetic field seven electromagnetic coils, each thinner then the Helmholtz coils used for previously mentioned tests, were placed along a F20T/12/CW production lamp within a water jacket as shown in Figure 4b.

Axial Field Configuration

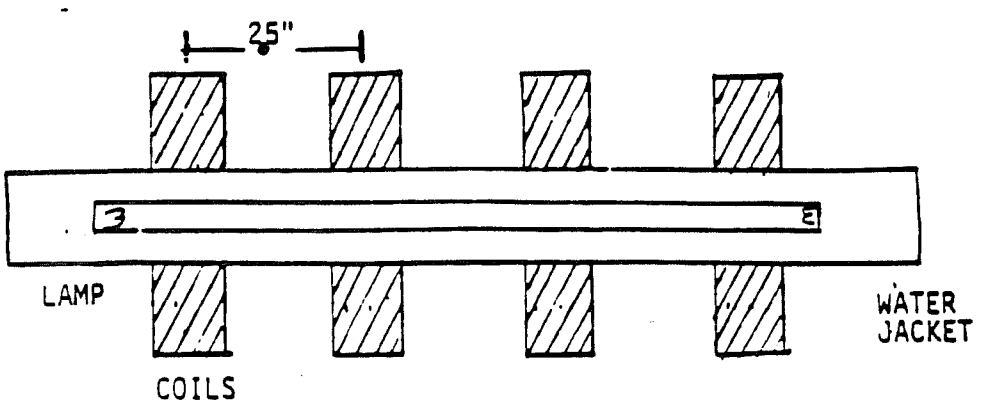

Fig. 4b

The axial field component varied by no more than 15% from coil center to intercoil midpoint. The test was carried out at 40°C, with relative efficacy recorded in the 1 meter sphere. Results are shown in Fig. 4c.

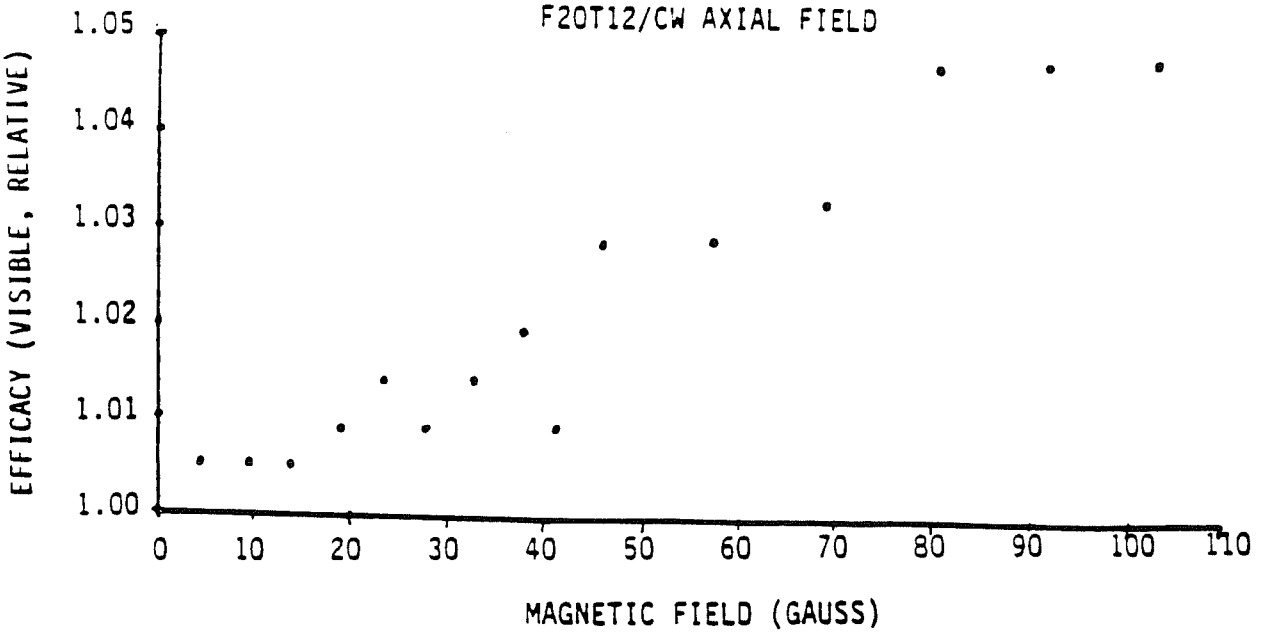

Figure 4c

Table 2 summarizes the type of magnetic field experiments and relative efficiency measurements carried out. Though it is clear from this work that magnetic fields can increase lamp efficiency the best practical application is not yet obvious. Furthermore, there are several factors which could be affecting the efficiency in the presence of a magnetic field. Further studies, through the measurement of the 253.7nm emitted hyperfine structure would help in the understanding of these factors.

Table 2
Summary of Magnetic Field Experiments

Localized Measurements		Integrating Sphere	
Transverse	Axial	Transverse	Axial
F40T/12 Uncoated	F40T/12 Uncoated	F40T/12 Strip Magnets	G8T/5
	F4T/5		F40T/12 End magnets
F4T/5 Moving slit		BENT T/5	F20T/12/CW
F4T/5 Line Intensities			

III. ISOTOPE LAMP INVESTIGATION

The principle data reduction for a quartz sectioned F40T/12 lamp was carried out. The data is comprised of lamp electrical operating parameters and relative U.V. output (253.7nm). One set of data was obtained for the lamp immersed in a waterbath and a second set obtained for a lamp whose cold spot temperature was controlled by a cooling coil. In the water bath setup, relative U.V. output was obtained via a 0.2 meter monochromator tuned to 253.7nm and a photomultiplier tube. The cooling coil measurements were carried out on an optical bench via a Fabry-Perot interferometer and a double pass 0.2 meter monochromator. Integrating the hyperfine structure spectrum gives the relative 253.7nm intensity.

In both the waterbath and interferometer measurements cold spot temperature and Hg isotopic distributions were varied. The major isotopic variation consists of increasing the ^{196}Hg concentration. All measurements were done in a single lamp thus avoiding possible lamp to lamp variation. After both sets of data were collected, the lamp mercury was analyzed via a mass spectrometer to determine the isotopic distribution. The ^{196}Hg concentration was determined to be 3.9%. At this point the isotopic distribution had been varied three times. Assuming equal doses of ^{196}Hg each time the isotopic distribution was changed in the lamp, (as well as no appreciable Hg loss) gives the following ^{196}Hg concentrations: 0.15% (natural Hg), 1.3%, 2.6% and 3.9%.

All data presented below was obtained for an arc current of 430 ma with the lamp operating off of a standard rapid start reference ballast. Both U.V. output and U.V. output per arc watt are plotted. The data is normalized to the values obtained at about 20°C cold spot temperature. This value was chosen because much below 20°C the lamp operation was not steady and also the presently available information

concerning isotope effects implies a negligible improvement in lamp operation at or below 20°C cold spot temperature for a F40T/12 lamp. Figures 5 and 6 show the U.V. data obtained. Figure 7 shows the corresponding electrical data. At 40°C our computer code predicts a 2.0 volt increase in arc voltage for a 3.3% ^{196}Hg concentration in a F40T/12 lamp operating at 430 ma arc current relative to natural mercury. This is about the change observed for the waterbath measurements. The general shape of the arc voltage versus cold spot temperature curves agree with data obtained by C. Jerome.[3]

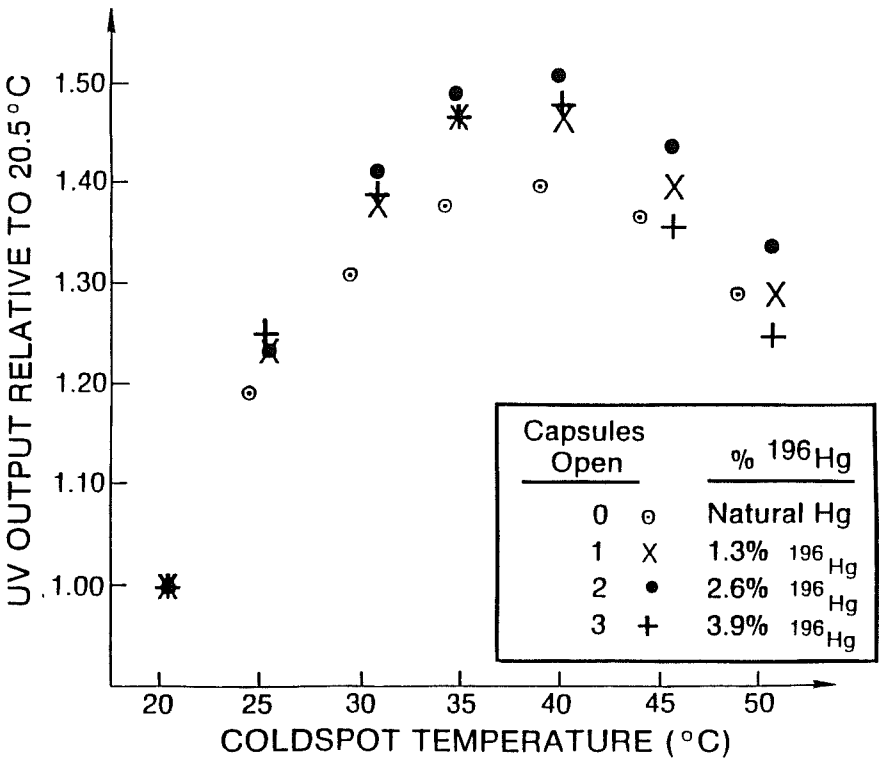

Figure 5. Variation of U.V. Output (253.7nm) as a function of Lamp Wall Temperature for different ^{196}Hg concentrations.

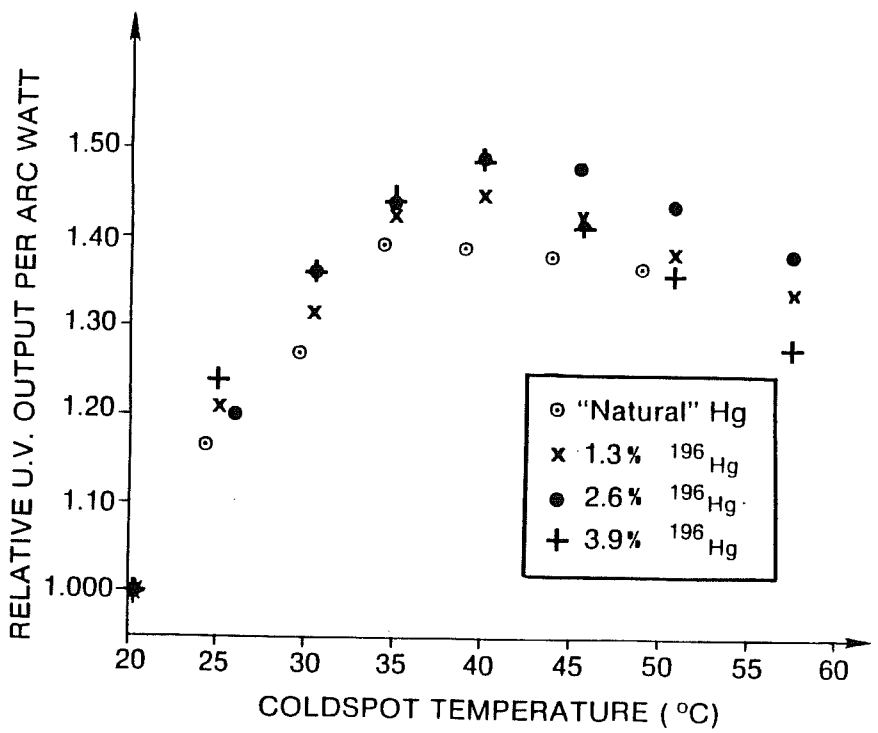

Figure 6. Variation of U.V. Output (253.7nm) per Arc Watt as a Function of Lamp Wall Temperature for Different ^{196}Hg Concentrations.

Variation of Arc Voltage versus Cold Spot Temperature for Different ^{196}Hg Concentrations. F40T/12 I_{arc} = 430 ma Waterbath Data.

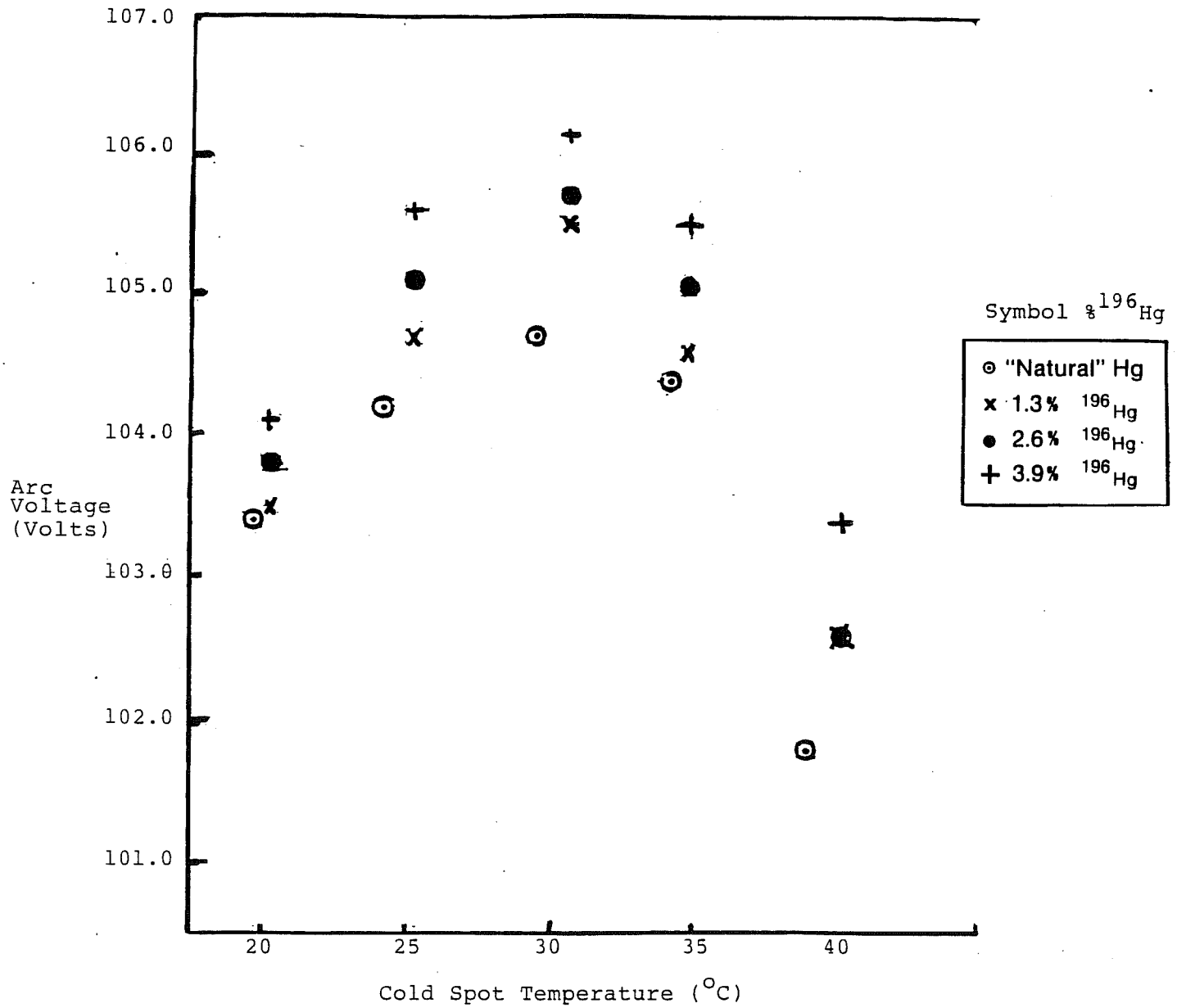

Fig. 7

Note however that integrating sphere measurements include end losses and one has to subtract that to compare it with the U.V. waterbath measurements. When that is done, the total integrating sphere measurements and U.V. waterbath data are in good agreement.

Note from Figures 5 and 6 that at 40°C UV/arc watt is the highest and same for 2.6% and 3.9% ^{196}Hg, while UV total output is higher by about 2% for the 2.6% ^{196}Hg than 3.9% ^{196}Hg. Under these conditions one would expect that the voltage for the 2.6% ^{196}Hg at 40°C would be somewhat higher than the voltage at 3.9% ^{196}Hg. The opposite is in fact true as can be seen from Figure 7. The voltage of the 3.9% ^{196}Hg is about 1% higher than the voltage at 2.6% ^{196}Hg at 40°C. In as much as this is within the measurement error it may also be suggesting that a 1% higher voltage across the leads is not translating into a 1% higher power into the positive column and possibly resulting in higher end losses. Another explanation may be that the phase factor is changing slightly when the voltage increases such that no additional power is being deposited into the positive column.

Relative U.V. emission measurements from a quartz sectioned F40T/12 lamp as a function of ^{201}Hg concentration and cold spot temperature were carried out. Three capsules containing 0.30 mg ^{201}Hg were opened and mixed with the initial 3.03 mg of natural Hg. Four separate sets of data were obtained, corresponding to initial natural Hg, 0.30 mg ^{201}Hg added, 0.60 mg ^{201}Hg added and 0.90 mg ^{201}Hg added. Cold spot temperature was varied from 20°C to 45°C and U.V. output was measured. Relative to 20°C natural Hg showed a maximum U.V. per arc watt output of 1.405 at 40°C whereas for the 0.30 and 0.60 mg of added ^{201}Hg, a maximum U.V. per arc watt output of 1.35 at 40°C was found. This decrease is not understood at this time. After the third capsule was opened, however, the maximum U.V. per arc watt output of 1.407 at 40°C was found. The estimated accuracy of these

measurements is ±1% so that at 0.90 mg of added ^{201}Hg, no difference was observed with respect to natural mercury.

In order to form small quantities of ^{201}Hg in the above experiment, we utilized isotopically "pure" (90% pure in case of ^{201}Hg) ^{201}HgO purchased from Oak Ridge National Lab. Hg was then electrolytically separated and deposited on Ni wire. The calibration of this dispensing procedure was greatly facilitated by using a potentiometric titration technique.

Potentiometric titration has been developed to quantitatively measure masses of small quantities of mercury or mercury ions. Here we discuss the use of this titration method to verify a mercury separation process used to form Hg into capsules.

Previously developed electroplating processes are used to reduce mercuric ion from solution onto a nickel wire as liquid mercury and then dispense this mercury from a sealed infrared absorbing capsule. Using a natural isotope composition HgO, the electroplating process has been tested as follows. Initial 10 ml solutions containing 0.510 mg Hg (as Hg^{++} ions) are used. Plating occurs for 3 to 5 hours at currents of 15 to 75 ma on a 1 inch long 0.020 inch diameter nickel wire. Using an I^- ion selective electrode, and a Ag/AgCl single junction reference electrode, potentiometric titration is carried out to measure the initial Hg^{++} concentration, the remaining Hg^{++} concentration after plating, and the amount of mercury transferred from the coated wire into a capsule.

The mercury transfer is carried out by placing the coated wire into a tube sealed at one end and then evacuating and partially backfilling the tube with Ar. The tube is tipped off and then placed almost completely into an oven heated to 400°C. One end of the tube is kept near room temperature so

the mercury vapor will condense into it. Once the 400°C temperature is reached the tube is quickly removed from the oven and the end of the tube containing the condensed Hg is sectioned off, forming a capsule, leaving the originally Hg coated wire in the other section of the tube.

The amount of Hg transferred can now be measured. The capsule is crushed open and about 10 ml HNO_3 (concentrated) is added to dissolve the liquid Hg. This is stirred for about 1 hour to assure the complete oxidation of Hg and this solution is then diluted with water which is titrated to find the Hg concentration. It is noted that in the titration process KI solution is added to the solution containing Hg^{2+} ions to form HgI_2 which is a highly insoluble salt. Very approximately, since the I^- ion selective electrode responds only to I^- ions, a strong electrode signal occurs only after all the Hg^{2+} is precipitated. (However, corresponding to the Nerst Equation and ion selective probe response function the change is not sudden). Figure 8a shows a typical titration curve for HgO. The "equivalence" point is best found utilizing a Gran plot in which the inflection point of the titration curve is determined by plotting $\Delta V/\Delta E$ versus V (change in titrant volume/probe voltage change versus total titrant volume added). The V intercept gives the equivalence point as shown in Figure 8b. Figure 8c is a Gran plot for the remaining solution after electrolytic separation and allows one to determine the extent of Hg removal from HgO solution and subsequent deposition on the nickel cathode. Table 3 shows the typical results of the Ni-Hg plating process for low plating currents. Higher currents are being investigated and appear to give higher separation factors without adversely affecting the plated mercury.

Table 3. Verification of Mercury Conversion Process.

Peak Current (ma)	Hg Remaining After Plating (mg)	Percent Hg Removed From Solution	Hg Measured After Distillation (mg)	Percent Lost Due To Distillation
15.5	0.10	79.5	0.398	1.4
13.5	0.14	72.4	0.329	9.1
13.0	0.15	69.0	0.309	9.6

T= 3 hours.
Initial Hg in each sample is 0.510 mg.

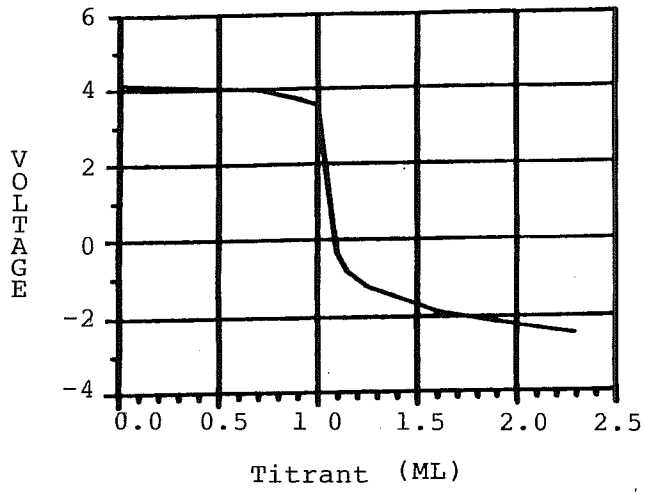

Figure 8a. **Titration Curve for Standard HgO Solution.**

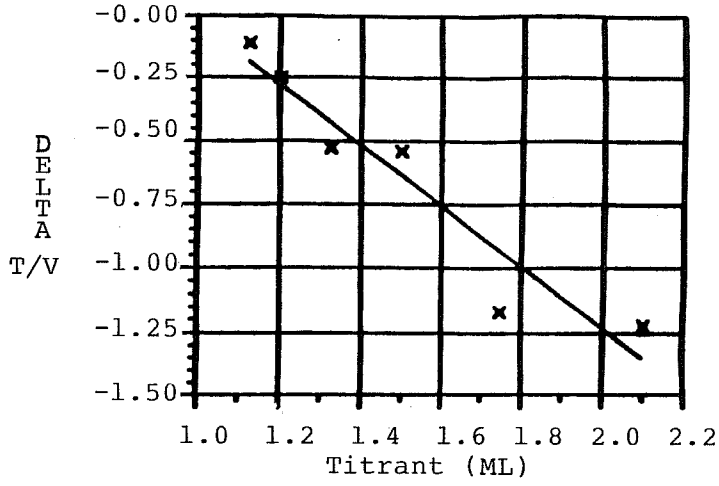

Figure 8b. **Gran Plot of Standard HgO Solution.**

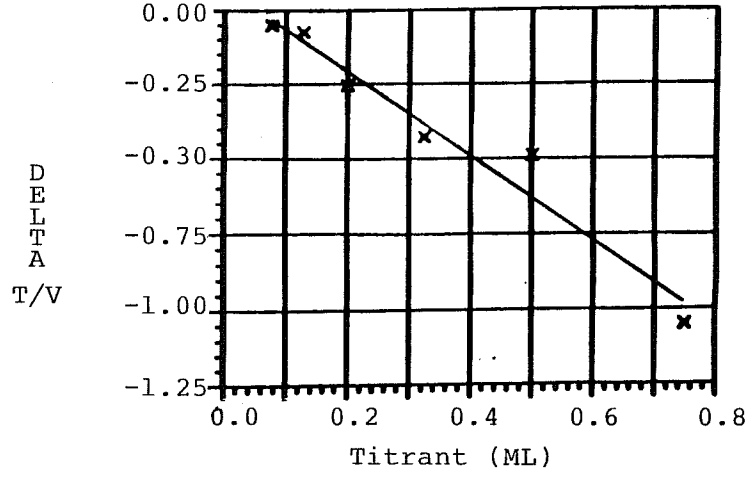

Figure 8c. **Gran Plot for Remaining Solution After Electrolyic Separation.**

IV. MODELING

Using the Holstein-Biberman integral equation we have studied the 253.7nm emitted hfs. Models were developed to obtain a best fit between the theoretical model and experimental Fabry-Perot interferometer data. One model utilized the analytic results of van Trigt[4] and was a useful tool to easily study various line shape phenomena. A more detailed analysis which included effects such as resonant energy transfer and hyperfine mixing was also developed and gave good agreement with the experimental data. Additionally, Monte Carlo calculations were carried out to determine the 253.7nm imprisonment time as well as emission efficiency for F40T/12 fluorescent lamp conditions.

The interferometer collection optics allows one to approximate the geometry of the F40T/12 lamp as a slab of thickness 2R. Van Trigt, following the formalism of the Holstein-Biberman integral equation, has found analytic solutions of the excited state density distribution for slab geometry in which kinetic excitation-de-excitation is included. The radiative transport equation[5] is used to determine the frequency distribution of the emerging radiation. Along a normal to the slab, the emerging radiation spectral distribution is given as:

$$I(u) = \text{constant} \cdot (k_o L)^{1/2} \left(\frac{k(u)\,L}{2}\right)^{1/4}$$

$$\times \exp\left(-\frac{k(u)L}{2}\right) \; I_{3/4}\left(\frac{k(u)L}{2}\right)$$

where k(u) is the frequency dependent absorption coefficient and k_o is k(u) evaluated at the center of the absorption line.

Additionally,

$$L = 2R = \text{slab thickness}$$

$$u = 2\left(\frac{\nu-\nu_o}{\Delta\nu_D}\right)$$

$\Delta\nu_D$ = Doppler full half width

$I_{3/4}$ = Modified Bessel function of order 3/4

An important parameter, A, is given as

$$A = \frac{\Delta\nu_L}{\Delta\nu_D}(\ln 2)^{1/2}$$

where $\Delta\nu_L$ = Lorentz full half-width

A represents the relative contributions of Doppler (thermal) and Lorentz (collisional) broadening and is used as a parameter in the Voigt emission and absorption profiles formed due to these line broadening processes. For F40T/12 lamps the approximate value of A is 0.01.

Fig. 9 shows the measured 253.7nm hfs for an F40T/12 lamp at $40^{o}C$ and $15^{o}C$ cold spot temperature. In order to match the calculations to the measured data one must include the effects of the instrumental broadening. This was carried out by convoluting the slab model calculations with an instrumental broadening function. The convolution function is the Airy function with an effective reflectivity determined from experimental data of R = 0.94. This folding function or instrumental function can be expressed as:

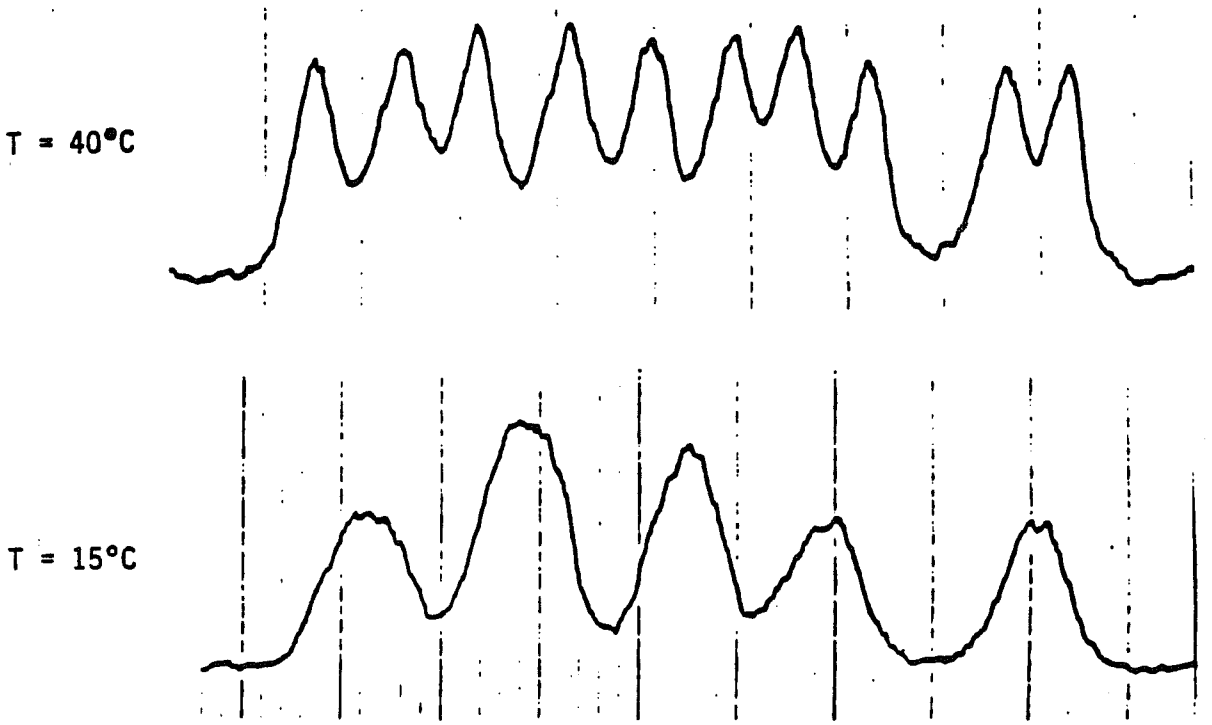

Figure 9. Measured Hyperfine Structure for Hg (253.7 nm) with "Natural" Isotopic Distribution.

$$I = \frac{Io}{1 + F \sin^2 \delta/2}$$

where $$F = \frac{4R}{(1-R)^2}$$

A variation of δ by 2π corresponds to 1 free spectral range or approximately 28.5 Doppler full half-widths ($40^{o}C$) for the interferometer settings used. If E represents the true shape of the hyperfine structure then the measured hyperfine structure is given as:

$$M(y) = \int E(x) \cdot I(y-x)dx \qquad \text{III-1}$$

where Equation III-1 represents the convolution of I and E. The range of integration is restricted by the fact that E is only measured over one free spectral range.

The integration of equation (III-1) has been carried out using the Digital Equipment Corporation subroutine QSF. Figures 10 and 11 show the calculated line shapes folded in with the convolution function for R=0.94 at cold spot temperatures of $15^{o}C$ and $40^{o}C$. The lines shapes are first calculated individually taking into account the statistical weight of each component. The frequency displacement of each of the six peaks is determined by the centroid method and no energy transfer or other atomic interaction is assumed which may affect the line shape. Also the overlapping wings of these components are summed to get the final non-convoluted, profile. This profile is then convoluted, following equation III-1 to obtain Figures 10 and 11.

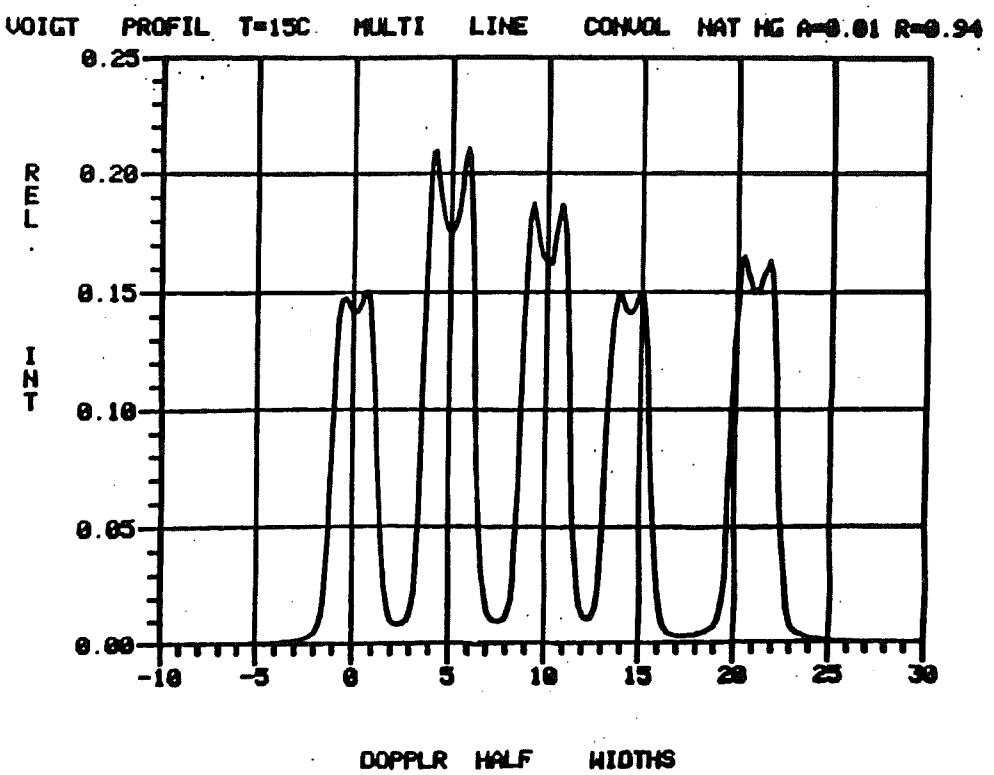

Figure 10

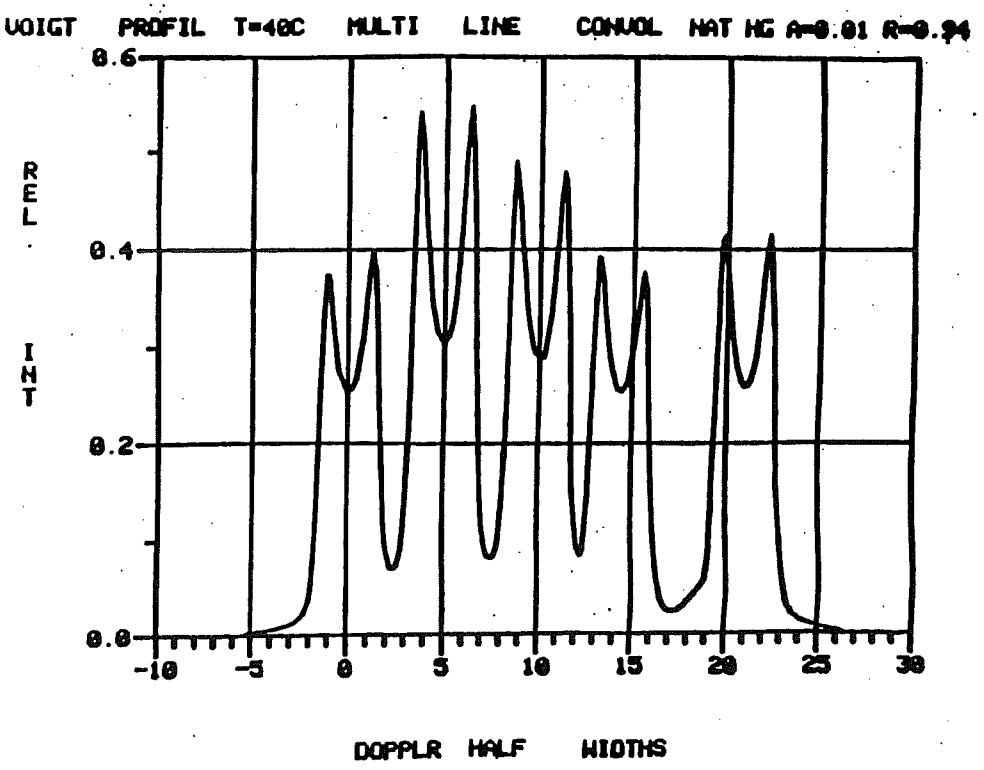

Figure 11

Comparing Figures 9, 10 and 11, we see that very little or no self-reversal is measured at $15^{o}C$ while it clearly shows in the calculated profile. There are several variables one could change in order to better match the profiles. For example, changing R to 0.60 better matches the $15^{o}C$ profiles but still is a poor match for profiles calculated at $40^{o}C$ where the self-reversal of each peak is measured to be much larger than calculated.

At this point, it is concluded that the van Trigt model, though relatively convenient to use, cannot predict the measured hfs.

Using a more complete formulation of the Holstein-Biberman equation, it has been found that the calculated profile of the 253.7 nm radiation is sensitive to the value of the rate constant $\langle v\sigma_t \rangle$ for the energy transfer between the line components.

Based on this sensitivity, we have determined the rate constant by fitting calculated hfs to experimental data. The instrumental profile has been taken in the form:

$$H(\nu) = \frac{1}{1 + F \sin^2 \sigma/s}$$

where $o \leq \sigma \leq \pi$ corresponds to the frequency range $o \leq \nu \leq 1.03 cm^{-1}$.

An important assumption in these calculations is that the excited atom spatial distribution is of the form

$$n(x) = n_o(1-Ax^2/R^2)$$

where x, R, and A are the distance from the axis, the tube radius, and a distribution parameter, respectively.

Calculations have been carried out for various values of the distribution parameter A, the instrumental parameter F and the rate constant $\langle v\sigma_t \rangle$. We found the best fit for the experimental data at A=1, F=400, and $\langle v\sigma_t \rangle = 3 \times 10^{-9}$ cm^3/sec. The calculated profile is shown in Figure 12.

CALCULATED HYPERFINE STRUCTURE

$t_{cold\ spot}=40^{o}C$

A = 1
F = 400
$\langle v\sigma_t \rangle = 3x10^{-9}cm^3/s$

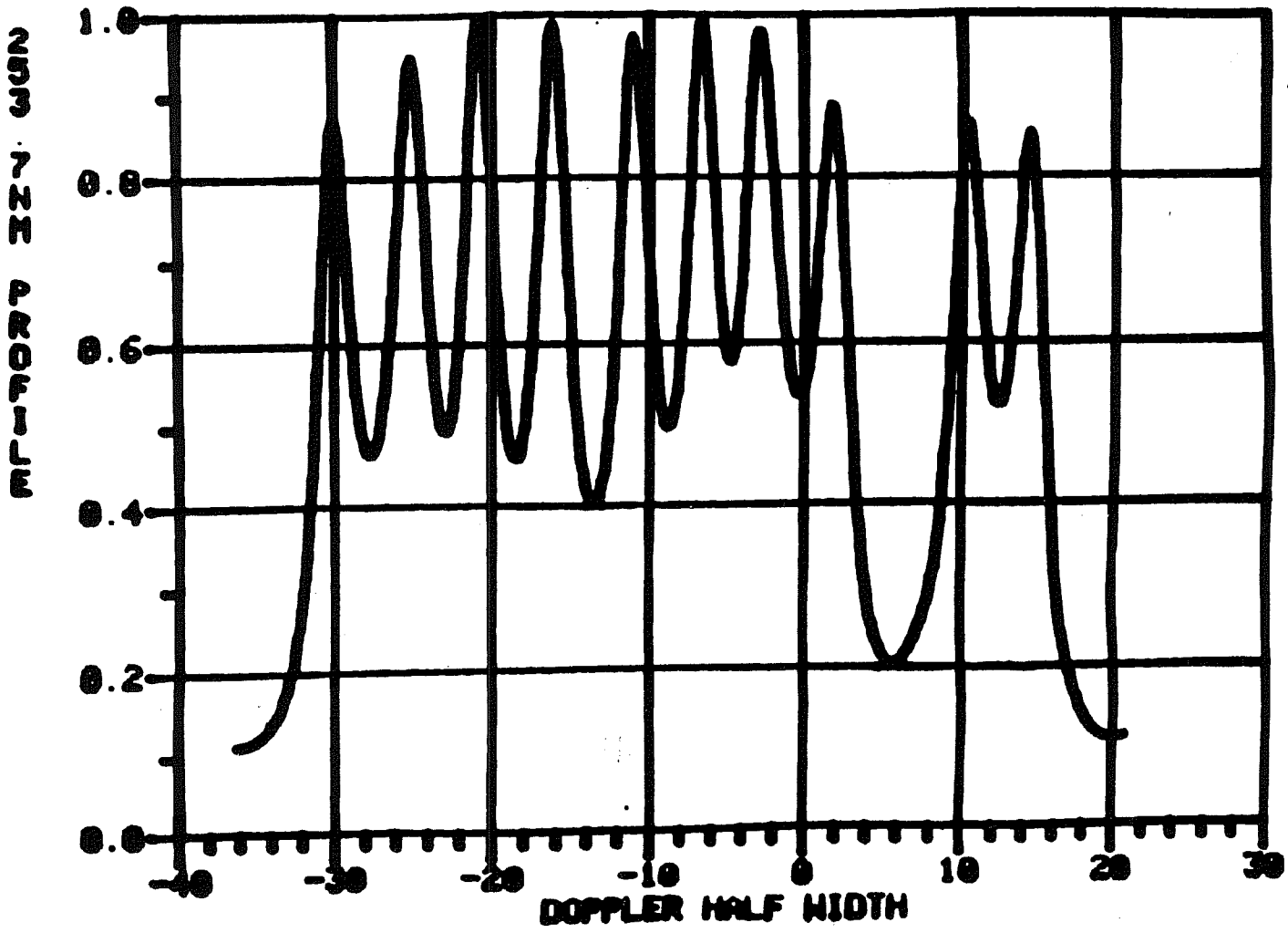

Figure 12

Considering the many parameters involved in the profile calculation and a possible experimental error, we estimate the possible error in the determined value of the rate constant to be equal to about 20%-30%.

The imprisonment time of the 253.7nm radiation as a function of the isotopic composition has also been calculated by the Monte-Carlo method. Calculations have been performed for F40T/12 lamp conditions.

The elementary type of atomic events need to be assigned a probability for these calculations. They are the probability of emitting a photon, Pe, the probability of transferring excitation energy from one atom to another, P_t, and the probability of an atom being quenched, Pq.

The probability of the excitation transfer to any particular isotopic or hyperfine component has been assumed proportional to the relevant isotope fraction and statistical weight. Also, the probabilities P_e, P_t and P_q satisfy the condition

$$P_e + P_t + P_q = 1$$

Probabilities P_t and P_q are determined by the equations:

$$P_t = \frac{R_t t}{1+R_t t+R_q t}$$

$$P_q = \frac{R_q t}{1+R_t t+R_q t}$$

Here t, R_t, R_q are the natural life time and rates of the excitation transfer and quenching for the mercury atom in the 6^3P_1 state, respectively. The rate of excitation transfer can be expressed as:

$$R_t = \langle v\sigma_t \rangle N_{Hg}$$

where σ_t, $\langle v\sigma_t \rangle$ and N_{Hg} are the excitation transfer cross-section, rate constant and the mercury number density, respectively. According to Reference 6, the value of $\langle v\sigma_t \rangle$ is 1×10^{-9} to 3.5×10^{-9} cm^3/sec.

The quenching of the 253.7 nm radiation is the cumulative result of many elementary processes as follows:

$$Hg(6^3P_{0,1,2}) + e \rightarrow Hg(6^1S_o) + e$$

$$Hg(6^3P_{0,1,2}) + e \rightarrow Hg(6^1P_1) + e$$

$$Hg(6^3P_{0,1,2}) + e \rightarrow Hg(6^3P_{0,1,2}) + e$$

$$Hg(6^3P_{0,1,2}) + e \rightarrow Hg^+ + e$$

$$Hg(6^3P_{0,1,2}) + Hg(6^3P_{0,1,2}) \rightarrow Hg_2^+ + Hg(6^1S_o) + e$$

Considering these processes, we have estimated the effective value of the quenching rate as $R_q \sim 10^4$ sec.

A photon can travel a certain free path between two absorption events. The photon free path can be defined as usual in terms of the absorption cross-section dependent on the frequency variation within the line profile. However, frequency dependence has not been considered in this particular version of the Monte-Carlo model. Instead, an average absorption cross-section σ_{abs} has been used. The value of σ_{abs} has been determined by fitting the calculated value of the imprisonment time to the experimental data[7] for conditions close to the conditions of the F40T/12 lamp. This resulted in:

$$\sigma_{abs} = 2 \times 10^{-13} cm^2$$

In order to have good statistical representation 10,000 photons are used initially in the calculational model

Results of calculations are presented in Tables 4 through 7. Calculational values of the imprisonment time for natural mercury are compared with experimental data[7] in Table 4. One can observe the good agreement for N_{Hg} x R tube of about $3.5 \times 10^{14} cm^{-2}$ (conditions of the F40T/12 lamp). The agreement is worse both for the lesser and greater mercury number densities. We believe this discrepancy is mainly due to the neglect of the photon frequency variation.

Tables 5 and 6 represent the calculated values of the imprisonment time and the relative efficiency as a function of the ^{196}Hg concentration. These data are in qualitative agreement with the identical data obtained employing the modified Holstein-Biberman approach. Both types of calculations predict the reduction of the imprisonment time and the increase of the efficiency with an enrichment by ^{196}Hg.

Table 7 contains the calculational data for the isotopic compositions enriched by ^{201}Hg. These data indicate reduction of imprisonment time by 2%-3% for the case of the excitation transfer rate constant equal to $\langle v\sigma_t \rangle = 1 \times 10^{-9}$ cm/sec. Increasing this constant to $\langle v\sigma_t \rangle = 3 \times 10^{-9}$ cm/sec. results in the disappearance of this gain. It is noted that we have observed the same trends with calculations using the Holstein-Biberman formulation.

In conclusion, one can say that the Monte-Carlo calculations confirm the results obtained by the modified Holstein-Biberman type calculations.

Table 4. Comparison of the Monte-Carlo Imprisonment Time with the Experimental Results of Alpert, McCoubrey and Holstein[5] for the Natural Mercury.

$N \times R_x \times 10^{14}$ cm^{-1}	(Monte-Carlo)	(Experimental)
1.30	2.07	3.1
1.95	3.79	5.8
3.25	8.78	9.3
6.50	29.80	20.4

Parameters used in the Monte-Carlo calculations:

$\sigma_{abs} = 2 \times 10^{-13}\ cm^2$.
$P_t = 0.062$/per event.
$\langle v\sigma_t \rangle = 3 \times 10^{-9}\ cm^3/sec$.
$R = 1.80cm$

Table 5. The Imprisonment Time Dependence on the Percentage of ^{196}Hg in an Isotope Mixture.

% ^{196}Hg	0.16%	1%	2%	3%	5%	7%	10%	15%
$P_t = 0.062$	1.000	0.947	0.891	0.849	0.782	0.771	0.747	0.746
$P_q = 0.021$	1.000	0.948	0.927	0.889	0.821	0.800	0.762	0.731

P_t = the probability of excitation transfer per one event.

$\langle v\sigma_t \rangle$ = the rate constant of excitation transfer.

T/12 conditions: R = 1.8 cm, P_{Hg} = 6mT, $T_{gas} = 313^{o}K$.

Table 6. The Relative Efficiency Dependence on the Percentage of ^{196}Hg in an Isotope Mixture.

% ^{196}Hg	0.16%	1%	3%	5%
$P_t = 0.062$ $P_q = 0.003$	1.000	1.0123	1.0340	1.0409
$P_t = 0.062$ $P_q = 0.001$	1.0000	1.0029	1.0130	1.0169
$P_t = 0.021$ $P_q = 0.003$	1.000	1.0095	1.0389	1.0409
$P_t = 0.021$ $P_q = 0.001$	1.0000	1.0001	1.0097	1.0137

P_t = the probability of excitation transfer per one event.

P_q = the probability of quenching per one event.

P_q = 0.001 corresponds to the quenching rate W ~9 x10^3 sec^{-1}

T/12 conditions: R = 1.8 cm, P_{Hg} = 6mT, T_{gas} = 313°K.

Table 7. Monte-Carlo Relative Efficiency Calculations for an Enrichment by ^{201}Hg

Added % ^{201}Hg	0.0%	5%	15%	25%	35%
$P_t = 0.062$ $P_q = 0$	1.000	1.024	1.017	1.022	1.020
$P_t = 0.021$ $P_q = 0$	1.000	0.987	0.968	0.972	0.981
$P_q = 0.021$	1.0000	1.0050	1.0043	1.0008	1.0047

V. MERCURY ISOTOPE SEPARATION

The isotope separation efforts concentrated on developing a reproducible and controllable process having an optimum enrichment and utilization factor. Diagnostics were developed to monitor the mercury flow rate and density, as well as a technique to measure the excitation line shape as a function of position within the reaction chamber. Calculations of the 253.7nm hfs were utilized to get a better understanding of the role of the excitation radiation in the enrichment process. A new, two-zone microwave 253.7 nm radiation source was developed in order to be able to optimize the primary excitation step in the enrichment process, and a cold spot controlled mercury vapor filter was developed and optimized. A number of process runs were carried out for the so-called direct enrichment process. Single pass ^{196}Hg concentrations of 2%-4% and have been obtained in a fairly reproducible manner.

Several diagnostics have been developed in order to get a better understanding and control of the enrichment process. The yield, enrichment, and utilization factors are defined as follows:

Q = total feedstock flow rate

Q_I = flow rate of I^{th} isotope in feedstock

Y = total yield = total rate of product deposit in collection area

Y_I = yield of I^{th} isotope in product

E_I = enrichment factor for I^{th} isotope in product

U_I = utilization factor for I^{th} isotope

Then these relations hold:

$$Q = \sum_I Q_I$$

$$Y = \sum_I Y_I$$

$$E_I = \frac{Y_I/Y}{Q_I/Q}$$

$$U_I = Y_I/Q_I$$

We measure Q using titration techniques as described in the "Isotope Lamp" section of this report. Q_I is inferred from the known feedstock isotope distribution and the relative Y_I values are determined via mass spectrometry. Y is also measured (see below) E_I and U_I are then found from the measured quantities as indicated in the above expression.

In order to determine Q, a second cold trap upstream and in series with the original trap, was added to the flow system. After the process parameters are set and the process reaches a steady state condition, liquid nitrogen is added to the second trap resulting in an accumulation of the effluent for a known period of time. The second trap is then removed from the system and the mercury separated from the effluent held within the trap. As mentioned, potentiometric titration is carried out in order to measure the amount of mercury collected. Knowing the collection time then infers the mass flow rate of mercury. The feedstock flow rate of each isotope, Q_I is inferred from the known feedstock isotope distribution.

We have estimated the total yield Y, by determining the amount of mercury separated from the product via an electrolytic process. The mercury is then isotopically analyzed via mass spectrometry to determine the relative yield of each isotope, Y_I. The enrichment factor for each

isotope E_I, in the product, is given as the relative yield divided by the relative feedstock flow rate for that isotope. The feedstock utilization factor for each isotope, U_I, is the ratio of Y_I to Q_I both of which are determined experimentally. This type of process parameter analysis is suitable for the so-called "direct" enrichment process. Applying this analysis and the upstream cold trap diagnostic to equivalent parameters as used in the early high enrichment run, we obtain the results in Table 8. We note that there is a large uncertainty in the feedstock utilization factor due to the method of estimating the yield.

Table 8. Summary of Results for ^{196}Hg Enrichment.

Single Pass Enrichment Factor	32
Yield	0.2 mg/hr
Feedstock Flow Rate	20 mg/hr
Feedstock Utilization Factor	0.3
HCl Flow Rate	100 sccm
C_4H_6 Flow Rate	100 sccm
Total Reactor Pressure	1 Torr

Another method of estimating the utilization factor which is very promising but just being developed, relies on the measurement of the isotopic distribution of the effluent. Figure 13 shows the mass spectra measurement carried out by GTE Waltham Laboratories, for a natural mercury standard, effluent sample, and corresponding direct enrichment run (yielding a concentration of 0.94% ^{196}Hg). The lower curves represent an enlargement of the ^{196}Hg peak region. From the numerical values of the relative peak heights as determined by GTE Waltham Laboratories and as noted in Figure 13, there is an apparent decrease in the ^{196}Hg concentration in the

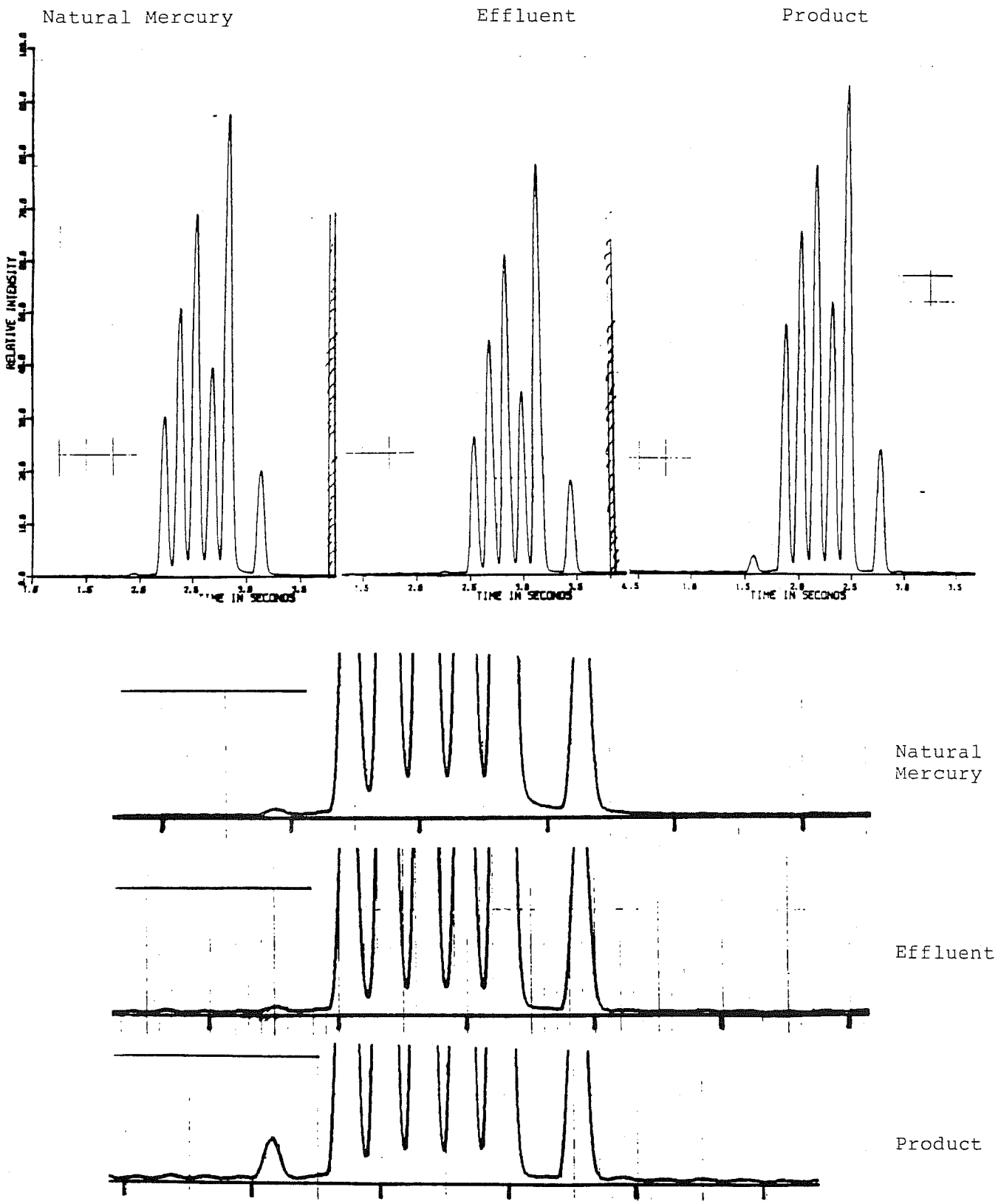
Natural Mercury
Effluent
Product
RELATIVE INTENSITY
TIME IN SECONDS
TIME IN SECONDS
TIME IN SECONDS
Natural Mercury
Effluent
Product

Figure 13

effluent. It is assumed that all the ^{196}Hg from the feedstock is either in the product or in the effluent. Then the fractional change in relative abundance of ^{196}Hg in the effluent with respect to the relative abundance of ^{196}Hg in the feedstock gives the utilization factor. This is seen more precisely by defining

F_I = effluent flow rate of I^{th} isotope and noting the assumption that

$$Q_I = F_I + Y_I$$

then

$$U_I = \frac{Y_I}{Q_I} = \frac{Q_I - F_I}{Q_I}$$

This technique is limited by how well the relative ^{196}Hg mass peak intensity can be measured. Background interference and non-zero mass spectrum peak wing heights appear to be limiting the accuracy of measurement.

Assuming a constant peak height displacement of ^{196}Hg of 0.237 -0.146 = 0.091, the effluent peak height of 0.217 represents a relative decrease of ^{196}Hg of 14% which corresponds to the utilization factor. The actual ^{196}Hg utilization factor may be higher because the background peaks are absent in the standard natural mercury spectra. Further work is being carried out by GTE Waltham Laboratories in order to improve this technique.

A special reactor chamber has been constructed to allow for measurement of the fraction of primary excitation radiation absorbed in order to measure the quantum efficiency of the photochemical reaction. This can be related to the absolute number of photons through the use of irradiance measurements carried out within the GTE Lighting Division. By knowing

the product formation rate, an average quantum efficiency can be determined.

A related figure of merit is the utilization of the available excitation photons. Depending on the cost of producing the excitation radiation and the quantum efficiency, this may be a critical parameter for a cost effective enrichment process.

As mentioned above, knowledge of mercury feedstock and effluent flow rates are important in determining the basic process parameters. One method to obtain these is via a second cold trap collection method as described above. Another technique which can be utilized to monitor the mercury flow rate is based on the relative transmission of the $Hg(6^3P_1 \rightarrow {}^1S_0)$ 253.7nm radiation through the effluent stream. This also gives a continuous monitoring diagnostic. A series of measurements were performed utilizing a natural mercury microwave source in which the attenuation measurements were used to observe changes in Hg flow rates. By calibrating the attenuation of the transmitted signal with respect to cold trap measurements, a continuous monitoring of the Hg flow rate can be carried out.

For these measurements, the probe is placed downstream of the throttle valve. Thus, it is reasonable to assume that for constant carrier gas flow through the system, the total pressure of the carrier gas is constant at the probe. Assuming that the mercury velocity is approximately equal to or proportional to the carrier gas velocity, one sees that the mercury velocity is constant at the transmission probe. Since changes in the mercury transmission signal represent changes in mercury line density, variation in the transmitted 253.7nm signal will then imply variation in Hg flow rate. In steady state with no losses the flow must be the same throughout the flow system. Thus, the transmission

probe can be used to monitor changes in Hg flow rates at the reaction chamber.

Figure 14a shows the variation in transmitted Signal I for different flow reactor total pressure, P, (using Argon) and Figure 14b is a plot of, J, versus 1/P and A versus 1/P where J is the measured Hg flow rate and

$$A = 1-I/I_o$$

J was measured for each value of P by determining the quantity of Hg collected in a cold trap. A second cold trap downstream of the first was used to pump away all residual Hg prior to the collection of Hg.

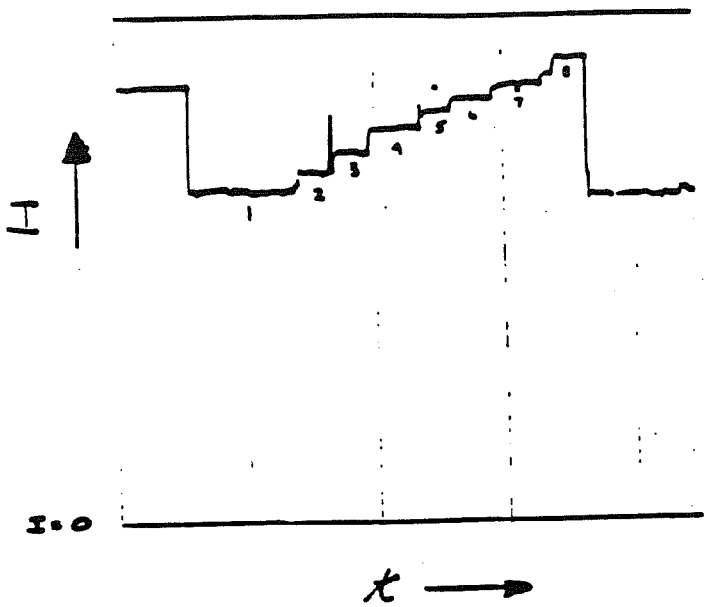

Figure 14a. Flow Monitor Output Versus Total Pressure

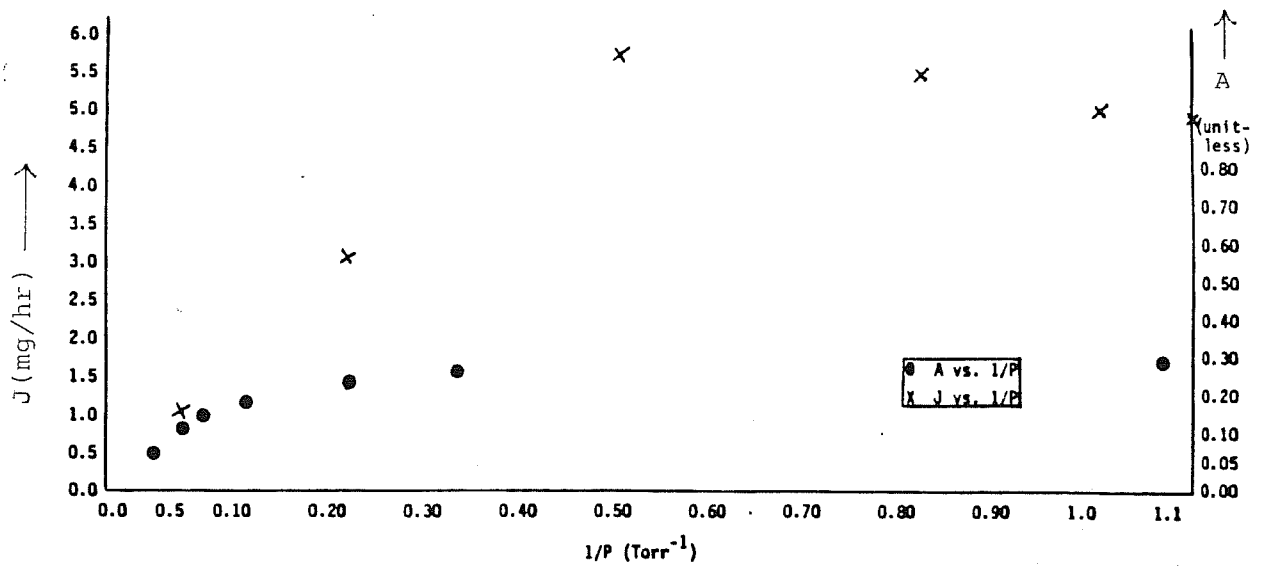

Figure 14b. J and A versus 1/P. Argon Carrier Gas 65S CCM

We have employed the fiber optic coupling scheme of the excitation source and interferometer to optimize a ^{196}Hg rf photochemical excitation lamp and natural Hg cold spot controlled filter. The fiber end at the interferometer was covered repeatedly in order to continually determine the zero signal level. This was carried out using a shutter in the form of a rotating disk with an annular semi-circle removed. Hydrogen and nitrogen were separately used in the filter in order to determine the best quenching gas. The maximum filter cold spot temperature obtainable with the present filter configuration is 24°C. Figure 15 shows the unfiltered ^{196}Hg rf lamp output (253.7 nm) and the effect of using the optimum filter conditions which are a 24°C cold spot temperature and a hydrogen fill pressure of 5 to 20 Torr. Figures 16, 17 and 18 show the results of varying several parameters on filter output. In addition to a higher cold spot filter temperature, the addition of ^{204}Hg and ^{198}Hg to the filter may improve the filtering process since these peaks do not appear as completely suppressed as other peaks. (See Figures 16 through 18.)

Using the optimized ^{196}Hg two-zone microwave lamp and natural mercury filter with controllable cold spot temperature, we investigated the direct enrichment process as a function of lamp and filter cold spot temperatures. Table 8 summarizes the up-to-date runs and corresponding ^{196}Hg enrichment for process conditions given in Table 10. In Table 9, the effect of lowering the lamp temperature and raising the filter temperature appears to give higher enrichment. This conclusion still needs to be investigated further because of the presence of a thin film coating the inner walls of the reactor vessel and the connecting downstream flow reactor section on which the product normally forms. The film was due to the silicone

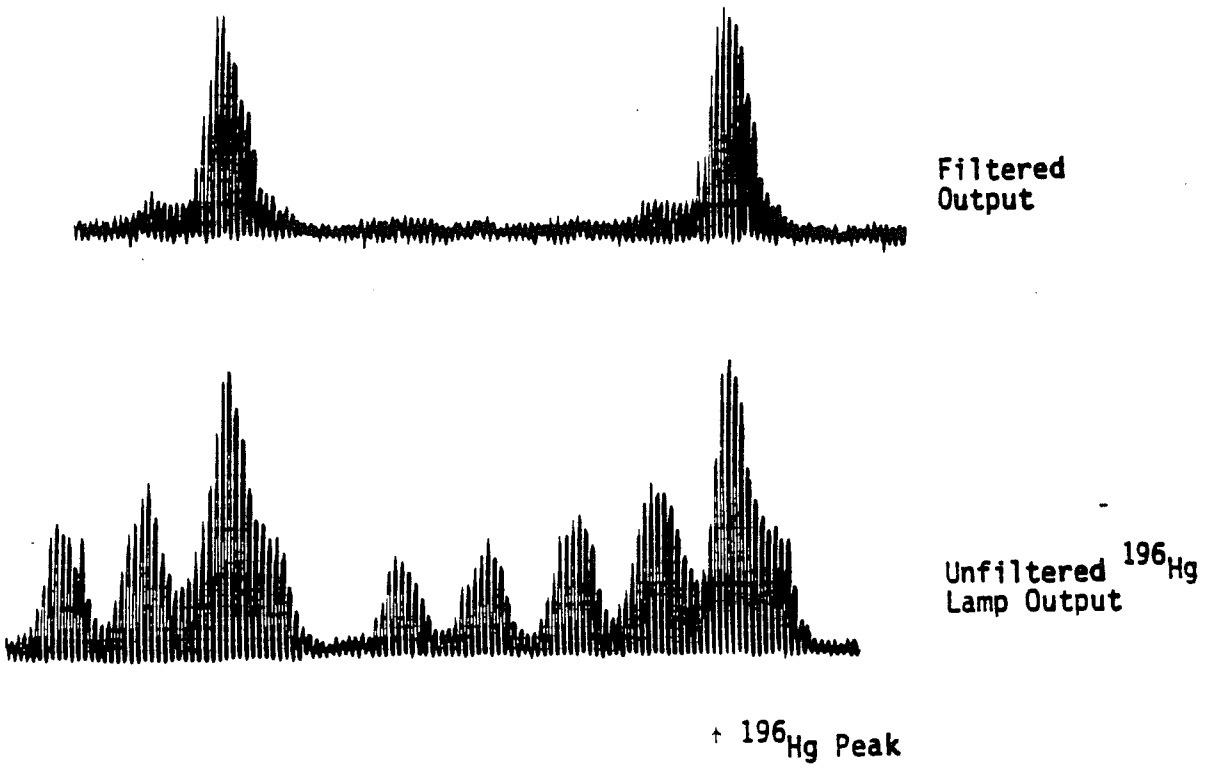

Figure 15. Effect of ^{N}Hg Filter on ^{196}Hg Lamp Output (253.7nm).

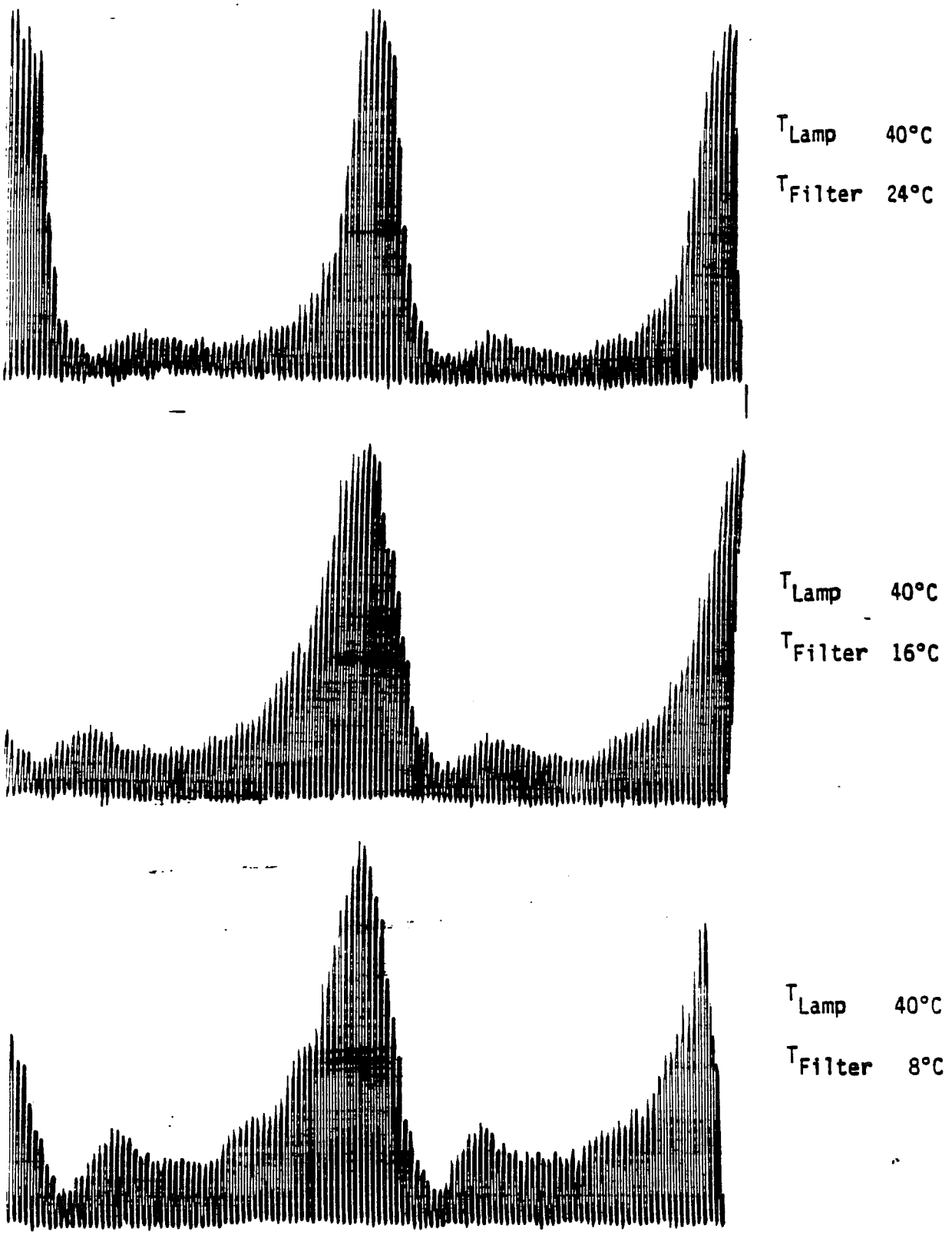

Figure 16. Effect of ^{N}Hg Filter Cold Spot Temperature on Transmitted HFS 10T Hydrogen ^{196}Hg RF Lamp.

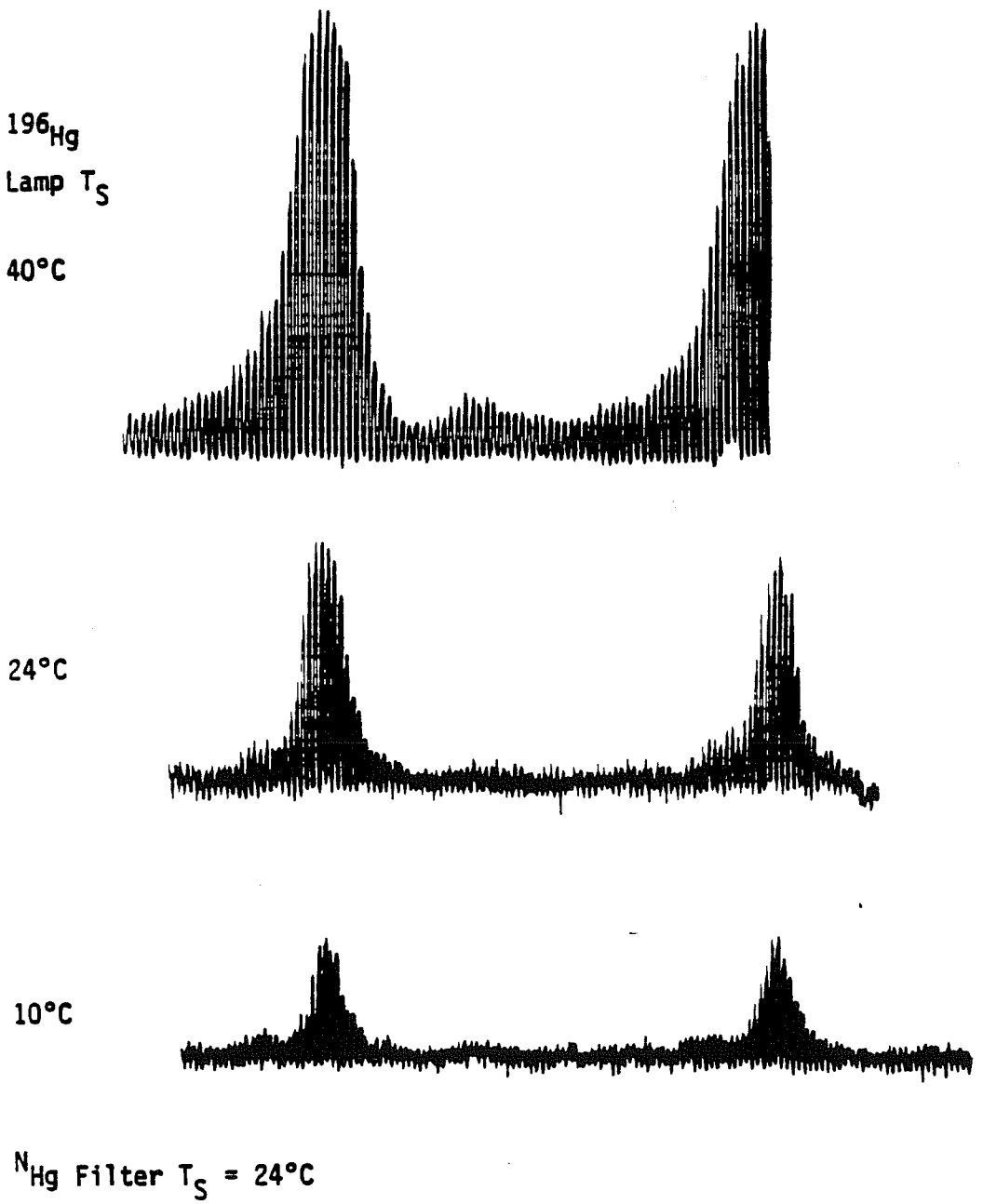

Figure 17. Variation of Transmitted Signal as a Function of Lamp Cold Spot Temperature.

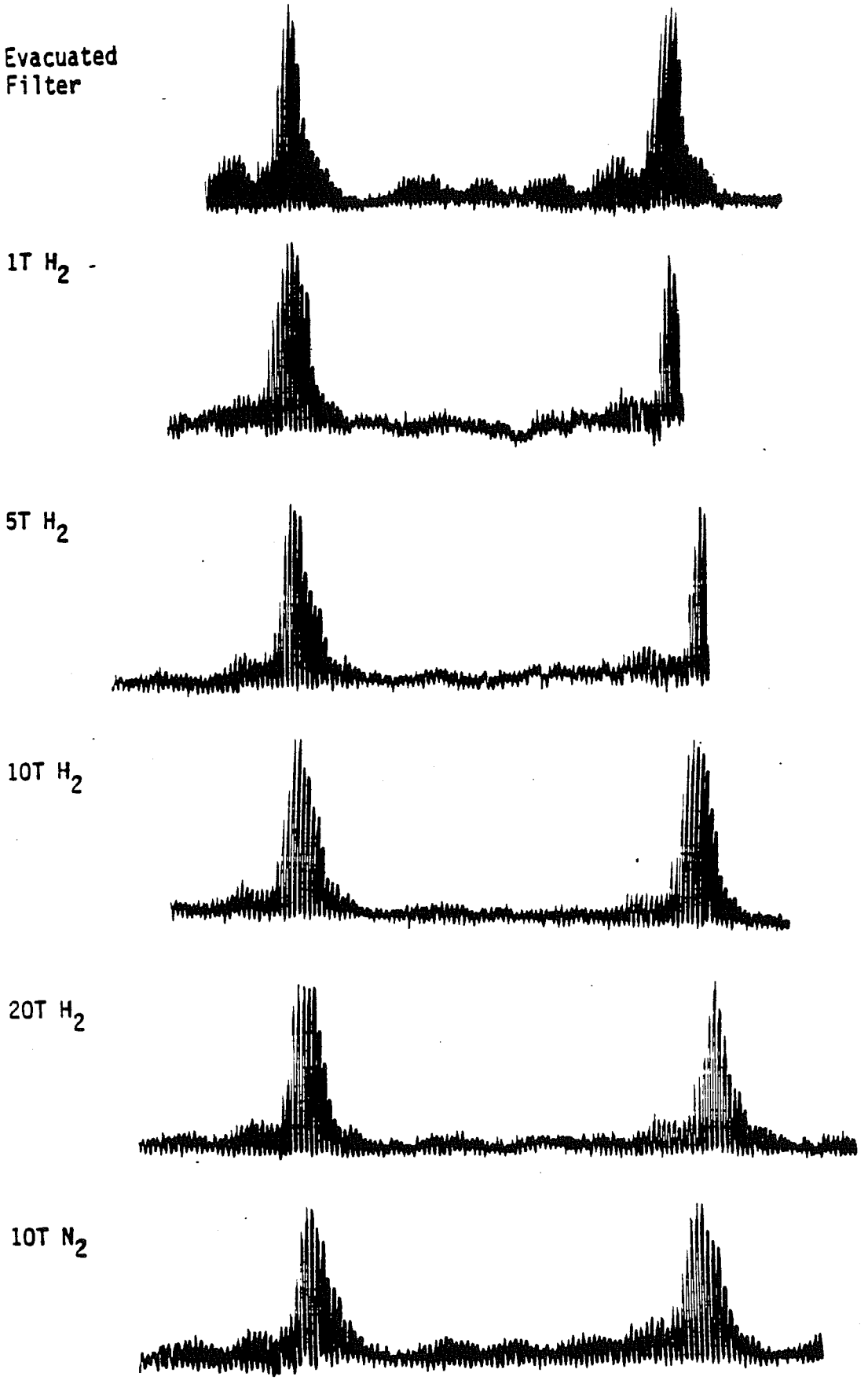

^{N}Hg Filter T_S = 24°C

^{196}Hg Lamp T_S = 20°C

Figure 18. Variation of Transmitted Signal as a Function of Fill Gas and Pressure.

Table 9. Variation of ^{196}Hg Enrichment versus Lamp and Filter Cold Spot Temperatures.

Run Number	^{196}Hg Lamp-T_c °C	N_{Hg} Filter T_c °C	^{196}Hg Product Concentration Reactor %	Downstream %	Comments
1	20	24	0.94	--	---
2	10	24	2.08	1.57	---
3	20	30	---	2.08	Surface Film
4	20	30	2.38	2.38	Reactor and Downstream Samples Combined

Table 10. Process Parameters for Direct Enrichment Runs.

Q_{HCl}	HCl Flow Rate	100 SCCM
Q_{HCl}	C_4H_6 Flow Rate	100 SCCM
P_{TOT}	Total Pressure	1.0 Torr
P_i	Input Power to Lamp	70 Watts
P_r	Reflected Lamp Power	34 Watts

seal grease that was transferred from the ground glass seal of a vacuum trap during cleaning. Removal of the film produced an apparently higher product formation rate as well as a more uniform product deposition on the inside of the reactor walls, as well as somewhat higher enrichment.

VI. SUMMARY AND FUTURE DIRECTION OF RESEARCH

To summarize our results to date we can make several statements with a high degree of confidence and point out future directions of research that in our opinion might prove to be very fruitful. First, our results in magnetic field experiments unequivocally demonstrate that there are efficiency improvements in fluorescent lamps due to the application of relatively modest transverse and axial magnetic fields. The level of these efficiency improvements, in most cases we have studied, are of the same order of magnitude as the isotope effect. In as much as we have determined that there is a certain amount of Zeeman splitting as a result of application of magnetic fields, we are not convinced that the efficiency increases are due entirely to this effect. We believe other effects, such as change in electron temperature, electric field and retardation of fast electrons could very well be contributing to the increase in efficiency. This is an area where further plasma studies would be very helpful.

Our investigations of the isotope effect in lamps have demonstrated the effect three ways. In phase 1 we demonstrated total light output and efficacy improvements due to isotopic enrichment. These were done in an integrating sphere under controlled temperature conditions. In this phase we carried out total U.V. as well as Fabry-Perot hyperfine structure measurements which basically explained the phenomenon as well as increased our level of confidence in the validity of our assertions.

Our understanding of the isotope effect has been augmented by two entirely different theoretical approaches. These are the analytical radiation transport method and the Monte-Carlo method. We developed a modified Holstein-Biberman formalism that takes into account energy transfer between

isotopes, overlap of different component line shapes and rare gas broadening mechanisms. With this approach we were able to predict the efficiency improvements as well as the hyperfine structure of the 253.7nm resonance line. The Monte-Carlo formalism basically accomplished similar results and confirmed the validity of the analytical approach. Using either approach we tried to find other isotopic mixtures that might have more favorable economics than ^{196}Hg enrichment. Both experimental, measurements and analytical and Monte Carlo calculations so far strongly suggest that a few percent ^{196}Hg is the most favorable enrichment scheme to obtain any measurable increase in efficiency. Furthermore, our studies strongly suggest that only ^{196}Hg enrichment without substantially altering the other isotopic compositions is necessary to obtain the increase in efficiency in fluorescent lamps. This naturally suggests that any isotope separation scheme will have to be highly selective, which means photon selective processes rather than mechanical or plasma processes (that yield a distribution of enriched isotopes) would be necessary to bring the discovery to a practical level.

In this phase of the program our photochemical isotope separation scheme has reached a greater degree of maturity. We have made progress in our understanding of the various factors that contribute to enrichment, scavenging, product yield and utilization (or stripping) factors. We have designed and successfully implemented an improved excitation source, product recovery process and flow and particle density diagnostics. We have devised a procedure to diagnose, in situ, the hyperfine structure of the excitation source, which is optimized for narrow ^{196}Hg emission. Furthermore, we have established reproducibility and increased the enrichment factor to 32 on a single pass.

At this point, however, our product yield is low enough (a few mg's/day) to make the process impractical for a large scale separation. Therefore we believe a scale-up project to separate about 0.5-1kg at a rate of about a few grams/day of a few percent ^{196}Hg enriched mercury would bring us much closer to moving the laboratory technology to the factory floor! We remain convinced that the photochemical process is reasonably well, even though not thoroughly, understood and potentially economic to warrant such a scale up effort.

VII. REFERENCES

1. R. W. Richardson and S. M. Berman, Third International Symposium on the Science and Technology of Light Sources, Toulouse FRANCE, April 1983.

2. J. H. Ingold and V. D. Roberts, Presentation in IES National Technical Conference, St. Louis, MO., Aug., 1984.

3. C. Jerome, Illuminating Eng. 51, 205 (1956).

4. Van Trigt, Phys. Rev. A1, 1314, (1970).

5. S. Chandrasekhar, Radiative Transfer, pg. 9 and pg. 354, Dover Publication (1960).

6. T. Holstein, D. Alpert, and A.O. McCoubrey, Phys. Rev. 85, 985 (1952).

7. D. Alpert, A.O. McCoubrey, T. Holstein, Phys. Rev. 76, 1257(1949).